Using a C^1 triangular finite element based on a refined model for analyzing buckling and post-buckling of multilayered plate/shell structures

F. Dau* O. Polit** M.Touratier***

*LAMEFIP/ENSAM, Esplanade des arts et métiers, 33405 Talence-France
**LMpX, 1 Chemin Desvallières, 92410 Ville d'Avray-France
***LMSP-UMR CNRS-ENSAM/ESEM, 151 Bd de l'Hopital, 75013 Paris-France

1 Introduction

Multilayered beam, plate and shell models and finite elements are needed in structural mechanics for analyzing, dimensionning and designing this kind of structures. In the field of multilayered shells where transverse shear stress effects are of great importance, many high order shell theories exist but very few numerical tools have been developped, see for example the review paper [4].

The aim of this work is to present a new finite element, simple to use, free from classical numerical problems and very efficient for computing both displacements and stresses for multilayered shell applications. This new C^1 shell finite element is based on the refined kinematic model given in [7] which incorporates :

- a cosine distribution for the transverse shear strains avoiding the use of shear correction factors,
- the continuity conditions between layers of the laminate for both displacements and transverse shear stresses,
- the satisfaction of the boundary conditions at the top and bottom surfaces of the shell,
- the use of only five independent generalized displacements (three translations and two rotations).

A conforming finite element method and high-order finite element approximations, Argyris interpolation for the transverse displacement and Ganev interpolation for membrane displacements and transverse shear rotations, are both retained in this work.

Some unavoidable geometric shell considerations are firstly presented to introduce necessary tools for shell description. In the second part of this paper, the shell model based on a refined kinematic approach is developped. The next part is dedicated to the finite element approximations and the present triangular finite element. Finally, numerical results, compared with experimental ones, are presented. Good results on classical tests for

multilayered plates and shells for both linear static and dynamic analysis have already been obtained using this new element. In this paper, critical buckling and post buckling problems are especially studied to show the efficiency of this new finite element for multilayered structures.

2 Geometric considerations

A shell $\mathcal{C}$ with a middle surface $\mathcal{S}$ and a constant thickness e is defined by, see [3] :

$$\mathcal{C} = \left\{ M \in \mathcal{R}^3 : \overrightarrow{OM}(\xi, \xi^3) = \vec{\Phi}(\xi) + \xi^3 \vec{a}_3; \xi \in \Omega; -\frac{1}{2}e(\xi) \leq \xi^3 \leq \frac{1}{2}e(\xi) \right\}$$

where the middle surface is described by a map $\vec{\Phi}$ from a parametric bidimensional domain Ω as :

$$\begin{array}{rcl} \vec{\Phi} \quad : \Omega \subset \mathcal{R}^2 & \longrightarrow & \mathcal{S} \subset \mathcal{R}^3 \\ \xi = (\xi^1, \xi^2) & \longmapsto & \vec{\Phi}(\xi) \end{array} \tag{1}$$

For a point on the shell middle surface, covariant base vectors are usually obtained as follows :

$$\vec{a}_\alpha = \vec{\Phi}(\xi^1, \xi^2)_{,\alpha} \quad ; \quad \vec{a}_3 = \frac{\vec{a}_1 \times \vec{a}_2}{||\vec{a}_1 \times \vec{a}_2||} = \vec{t}_3 \tag{2}$$

In Eq. (2) and further on, latin indices $i, j, \ldots$ take their values in the set $\{1, 2, 3\}$ while greek indices $\alpha, \beta, \ldots$ take their values in the set $\{1, 2\}$. The summation convention on repeated indices and the classic notation $(\ \ )_{,\alpha} = \dfrac{\partial(\ \ )}{\partial \xi^\alpha}$ are used.

For any point of the shell, covariant base vectors are now deduced as :

$$\vec{g}_\alpha = \vec{r}(\xi^1, \xi^2, \xi^3)_{,\alpha} = (\delta_\alpha^\beta - \xi^3 b_\alpha^\beta)\vec{a}_\beta = \mu_\alpha^\beta \vec{a}_\beta \quad \text{and} \quad \vec{g}_3 = \vec{a}_3 \tag{3}$$

The mixed tensor m_α^β must also be introduced and is defined by the relation :

$$m_\alpha^\beta = (\mu^{-1})_\alpha^\beta = \frac{1}{\mu}\{\delta_\alpha^\beta + \xi^3(b_\alpha^\beta - 2H\delta_\alpha^\beta)\} \tag{4}$$

where $\mu = det(\mu_\alpha^\beta) = 1 - 2H\xi^3 + (\xi^3)^2 K$; $H = \frac{1}{2}tr(b_\alpha^\beta)$; $K = det(b_\alpha^\beta)$.

Therefore, the covariant metric tensor $a_{\alpha\beta}$, covariant $b_{\alpha\beta}$ and mixte b_α^β curvature tensors can be defined. These tensors and some relations between them are recalled hereafter :

$$\begin{array}{rclcrcl} a_{\alpha\beta} & = & a_{\beta\alpha} = \vec{a}_\alpha . \vec{a}_\beta & \qquad & \vec{a}_\alpha & = & a_{\alpha\beta}\vec{a}^\beta \\ b_{\alpha\beta} & = & b_{\beta\alpha} = -\vec{a}_\alpha . \vec{a}_{3,\beta} & & b_\alpha^\beta & = & a^{\beta\gamma} b_{\gamma\alpha} \end{array} \qquad a = det(a_{\alpha\beta}) \tag{5}$$

Finally, the surface element dS and the volume element dV are classically given by :

$$\begin{array}{rcl} dS & = & \sqrt{a} d\xi^1 d\xi^2 \\ dV & = & \mu dS d\xi^3 \end{array} \tag{6}$$

All these relations are classic and more details in order to obtain the Christoffel symbols and other differential geometric entities could be found in Bernadou [3].

3 The shell model

3.1 The displacement field

Let us denote by $u_i^{(k)}(\xi^1, \xi^2, \xi^3 = z, t)$, $i \in \{1, 2, 3\}$ the curvilinear components of the displacement field associated with the contravariant base vectors $\vec{a}^i$.

The refined displacement field is based on continuity requierements from [2] and follows classical plate/shell assumption $\sigma_{33} = 0$. In a layer (k), it is expressed as [5] :

$$\left\{ \begin{array}{lcl} u_1^{(k)}(\xi^1, \xi^2, z, t) & = & \mu_1^\alpha \; v_\alpha(\xi^1, \xi^2, t) - z \; v_{3,1}(\xi^1, \xi^2, t) + F_1^{\alpha(k)}(z) \; \gamma_\alpha^0(\xi^1, \xi^2, t) \\ u_2^{(k)}(\xi^1, \xi^2, z, t) & = & \mu_2^\alpha \; v_\alpha(\xi^1, \xi^2, t) - z \; v_{3,2}(\xi^1, \xi^2, t) + F_2^{\alpha(k)}(z) \; \gamma_\alpha^0(\xi^1, \xi^2, t) \\ u_3^{(k)}(\xi^1, \xi^2, z, t) & = & v_3(\xi^1, \xi^2, t) \end{array} \right. \tag{7}$$

where t is the time and the classical summation on repeated indices is used. In Eq. (7), v_i are displacements of a point on the middle surface and γ_α^0 is the transverse shear strain at $z = 0$, while $F_\beta^{\alpha(k)}$ are functions of the normal transverse co-ordinate z defining the distribution of the transverse shear stresses through the thickness. They are defined by :

$$\begin{array}{ll} F_1^{1(k)}(z) = f_1(z) + {g_1}^{(k)}(z) & F_1^{2(k)}(z) = {g_2}^{(k)}(z) \\ F_2^{1(k)}(z) = {g_3}^{(k)}(z) & F_2^{2(k)}(z) = f_2(z) + {g_4}^{(k)}(z) \end{array} \tag{8}$$

In Eq. (8), the thickness functions $f_1, f_2, {g_1}^{(k)}, \ldots, {g_4}^{(k)}$ depend on coefficients $a_i^{(k)}, d_i^{(k)}, b_{44}, b_{55}$ and trigonometric functions as follows :

$$\begin{array}{l} f_1(z) = f(z) - \frac{e}{\pi} b_{55} f'(z) \\ f_2(z) = f(z) - \frac{e}{\pi} b_{44} f'(z) \\ {g_i}^{(k)}(z) = {a_i}^{(k)} z + {d_i}^{(k)} \quad i = 1, 2, 3, 4. \quad \text{and} \quad k = 1, 2, 3, \ldots, N. \end{array} \tag{9}$$

with $f(z) = \dfrac{e}{\pi} \sin \dfrac{\pi z}{e}$ and $f'(z)$ stands for $f(z)$ derivative with respect to z co-ordinate. N represents the number of layers.

These coefficients are determined from the boundary conditions on the top and bottom surfaces of the shell, and from the continuity requirements at the layer interfaces for displacements and stresses, see Béakou [2].

From Eq. (7), classical shell models can be deduced :

- the classical shell theory (Koïter theory), called CST model with :

$$f_1(z) = f_2(z) = 0 \quad \text{et} \quad g_i^k(z) = 0$$

- the first order shear deformation theory (Naghdi theory), called FSDT model with :

$$f_1(z) = f_2(z) = z \quad \text{et} \quad g_i^k(z) = 0$$

Hereafter, the superscript (k) for ${u_\alpha}^{(k)}$ components is omitted in order to simplify the finite element description.

3.2 The strain field

After some algebraic calculations, the covariant strain tensor components are obtained in the local contravariant basis $\vec{a}^i$ as follows :

$$\epsilon = \epsilon_{ij}(a^i \otimes a^j) \quad \text{with}$$

$$\begin{aligned} 2\epsilon_{\alpha\beta} &= \frac{1}{\mu}\Big(\epsilon^0_{\alpha\beta} + \epsilon^0_{\beta\alpha} + F^\nu_\alpha(z)\,\epsilon^1_{\nu\beta} + F^\nu_\beta(z)\,\epsilon^1_{\nu\alpha} + G^\nu_\alpha(z)\,\epsilon^2_{\nu\beta} + G^\nu_\beta(z)\,\epsilon^2_{\nu\alpha} \\ &\quad + z\Big\{(b^\lambda_\beta - 2H\delta^\lambda_\beta)\,(\epsilon^0_{\alpha\lambda} + F^\nu_\alpha(z)\,\epsilon^1_{\nu\lambda} + G^\nu_\alpha(z)\,\epsilon^2_{\nu\lambda}) + \\ &\quad (b^\lambda_\alpha - 2H\delta^\lambda_\alpha)\Big(\epsilon^0_{\beta\lambda} + F^\nu_\beta(z)\,\epsilon^1_{\nu\lambda} + G^\nu_\beta(z)\,\epsilon^2_{\nu\lambda}\Big)\Big\}\Big) \\ 2\epsilon_{\alpha 3} &= F^{\nu'}_\alpha(z)\,\gamma^0_\nu \end{aligned} \tag{10}$$

with $G^\nu_\alpha(z) = F^\nu_\alpha(z) - \delta^\nu_\alpha\ z$ and $F^{\nu'}_\alpha(z)$ stands for $F^\nu_\alpha(z)$ derivative with respect to z co-ordinate.

By convenience, the following notations have been introduced in Eq. (10) to caracterize the mechanical effects :

membrane strain : $\epsilon^0_{\alpha\beta} = v_{\alpha|\beta} - b_{\alpha\beta}v_3$

bending strain 1 : $\epsilon^1_{\alpha\beta} = \beta_{\alpha|\beta}$

bending strain 2 : $\epsilon^2_{\alpha\beta} = b^\lambda_\alpha v_{\lambda|\beta} + b^\lambda_{\alpha|\beta}v_\lambda + v_{3|\alpha\beta}$

transverse shear strain : $\gamma^0_\alpha = \beta_\alpha + b^\beta_\alpha v_\beta + v_{3,\alpha}$

where the notation $_{|\beta}$ stands for the covariant derivation with respect to the ξ^β curvilinear co-ordinate.

4 The finite element approximation

4.1 The discrete weak form of the boundary value problem

The discrete formulation of the shell boundary value problem in linear elasticity is deduced from the following functional :

$$a(\vec{u}^h, \vec{u}^{*h})_{\cup\Omega_e} = f(\vec{u}^{*h})_{\cup\Omega_e} + F(\vec{u}^{*h})_{\cup\mathcal{C}_e}\ , \quad \forall \vec{u}^{*h} \tag{11}$$

where $\cup\Omega_e$ is the triangulation of the multilayered structure and $\cup\mathcal{C}_e$ is the edge of the meshed structure. In addition, $\vec{u}^h$ is the finite element approximation of the displacement field $\vec{u}$ given by Eq. (7) and $\vec{u}^{*h}$ is the finite element approximation of the corresponding virtual velocity field $\vec{u}^*$. Linear functions f and F represent the body (including inertia terms) and surface loads, actually surface and line loads respectively, due to the integration performed throughout the thickness in Eq. (11). The superscript h introduced in Eq. (11) indicates the finite element approximation. It is also used for finite element approximation of the generalized displacements in Eq. (7), denoted by ${v_i}^h$ and ${\theta_\alpha}^h$ with $i = 1, 2, 3$ and $\alpha = 1, 2$.

The geometry of the shell is approximated by the classical three node triangular finite element.

4.2 The generalized displacement approximations

In a conforming finite element approach, the displacement field, given by Eq. (7) indicates that ${v_3}^h$ must be approximated by a C^1-continuous function. The other generalized displacements ${v_\alpha}^h$ and ${\theta_\alpha}^h$ have to be defined in the Sobolev space $H^1(\Omega_e)$. Those functions must be at least C^0-continuous.

Therefore, Argyris interpolation for the deflexion and the Ganev interpolation for the other generalized displacements are used. Note that the Argyris interpolation is exactly of continuity C^1 and the Ganev interpolation involves a semi-C^1 continuity which is not needed here. Due to very long expressions for these interpolations, the reader is referred to either the original papers [1] and [6] or a recent book [3].

The degrees of freedom associated with one finite element in the local curvilinear basis are given as :

- for a corner node :

$$\begin{array}{cccccc} v_1 & v_{1,1} & v_{1,2} & v_2 & v_{2,1} & v_{2,2} \\ v_3 & v_{3,1} & v_{3,2} & v_{3,11} & v_{3,22} & v_{3,12} \\ \theta_1 & \theta_{1,1} & \theta_{1,2} & \theta_2 & \theta_{2,1} & \theta_{2,2} \end{array} \tag{12}$$

- while, for a mid-side node :

$$\begin{array}{cccc} v_1 & v_{1,n} & v_2 & v_{2,n} \\ v_{3,n} & & & \\ \theta_1 & \theta_{1,n} & \theta_2 & \theta_{2,n} \end{array} \tag{13}$$

where $p_{,n}$ is the derivative with respect to the normal direction of the edge element.

Then, having derivatives in the previous set of degrees of freedom (dof), the following methodology is used to prescribe kinematic boundary conditions.

For a given p function with the condition $p(\xi^1 = 0, \xi^2) = 0$ to satisfy $\forall \xi^2$, then the first order derivatives become :

$$\begin{aligned} p_{,1}(0,\xi^2) &= \lim_{h\to 0} \frac{p(h,\xi^2) - p(0,\xi^2)}{h} \neq 0 \\ p_{,2}(0,\xi^2) &= \lim_{h\to 0} \frac{p(0,\xi^2+h) - p(0,\xi^2)}{h} = 0 \end{aligned} \tag{14}$$

and so on for the second order derivatives.

4.3 The elementary matrices

4.3.1 The stiffness matrix

The elementary stiffness matrix $[K_e]$ is obtained by computing the bilinear form given in Eq. (11) at the elementary level as :

$$\begin{aligned} a(\vec{u}^h, \vec{u}^{*h})_{\Omega_e} &= \int_{\Omega_e} \int_{-e/2}^{e/2} \left[\epsilon_e^{*h}\right]^T \left[\bar{C}^{(k)}\right] \left[{\epsilon_e}^h\right] \mu dz \sqrt{a} d\Omega_e \\ &= \int_{\Omega_e} \left[E_e^{*h}\right]^T \left(\int_{-e/2}^{e/2} [B_e]^T \left[\bar{C}^{(k)}\right] [B_e] \mu dz \right) \left[{E_e}^h\right] \sqrt{a} d\Omega_e \\ &= \int_{\Omega_e} \left[E_e^{*h}\right]^T [A_e] \left[{E_e}^h\right] \sqrt{a} d\Omega_e \\ &= [Q_e^*]^T [K_e] [Q_e] \end{aligned} \tag{15}$$

Using the displacement field $\vec{u}$ in Eq. (7) and the strain components in Eq. (10), the matrix $[B_e]$ can easily be deduced. It is computed by the following relation :

$$[B_e] = [Ep][Geo] \tag{16}$$

In the above expression of matrix $[B_e]$, $[Ep]$ is a matrix containing thickness functions of the co-ordinate z whereas $[Geo]$ is a matrix including only differential geometry entities such as metric tensor, curvature tensor and Christoffel symbols (see Bernadou [3]).

The matrix $[{E_e}^h]$ (identically for $[E_e^{*h}]$ adding the asterisk superscript), which may be seen as a generalized displacements matrix, is given by :

$$\begin{aligned}\left[{E_e}^h\right]^T = \big[\; & {v_1}^h \quad {v_1}^h{}_{,1} \quad {v_1}^h{}_{,2} \quad \vdots \quad {v_2}^h \quad {v_2}^h{}_{,1} \quad {v_2}^h{}_{,2} \quad \vdots \\ & {v_3}^h \quad {v_3}^h{}_{,1} \quad {v_3}^h{}_{,2} \quad {v_3}^h{}_{,11} \quad {v_3}^h{}_{,12} \quad {v_3}^h{}_{,22} \quad \vdots \\ & {\theta_1}^h \quad {\theta_1}^h{}_{,1} \quad {\theta_1}^h{}_{,2} \quad \vdots \quad {\theta_2}^h \quad {\theta_2}^h{}_{,1} \quad {\theta_2}^h{}_{,2} \; \big]\end{aligned} \tag{17}$$

The finite element approximations, defined at the above section 4.2, are directly used to express the matrix $\left[{E_e}^h\right]$ as a function of the elementary degrees of freedom vector $[Q_e]$ (see Eq. (12) and Eq. (13)).

Finally, $[A_e]$ contains the material behaviour matrix for a multilayered finite element, resulting from the integration with respect to the thickness co-ordinate, and differential geometry entities such as metric, curvature, Christoffel symbols, ...

4.4 Extension to the geometric non linearity

The multilayered structure is now considered in a Total Lagrangian configuration, so that its mesh is denoted $\cup\Omega_e(0)$ with edge $\cup C_e(0)$ where (0) indicates the initial (fixed) configuration used. Lagrangian co-ordinates will hereafter be written ξ^i as previously. The discrete boundary value problem "stated" above for linear analysis Eq. (11) is therefore formulated by the following Total Lagrangian functional available for non-linear analysis :

$$J(\vec{u}^h, \vec{u}^{*h})_{\cup\Omega_e(0)} = a(\vec{u}^h, \vec{u}^{*h})_{\cup\Omega_e(0)} - f(\vec{u}^{*h})_{\cup\Omega_e(0)} - F(\vec{u}^{*h})_{\cup\mathcal{C}_e(0)} = 0 \; , \quad \forall \vec{u}^{*h} \tag{18}$$

Absence of followed forces is considered here. Thus, the main feature of the non-linear formulation is incorporated into the virtual internal power and the following expression is obtained :

$$a(\vec{u}^h, \vec{u}^{*h})_{\Omega(0)} = \int_{\Omega(0)} \int_{-e/2}^{e/2} \left[\epsilon_e^{*h}\right]^T \left[\bar{C}^{(k)}\right] \left[{\epsilon_e}^h\right] \mu dz \sqrt{a} d\Omega_e(0) \tag{19}$$

All the quantities in Eq. (19) refer to the initial (fixed) configuration. Virtual strain rates and strains can be split into their linear (index L) and non-linear (index NL) parts as follows :

$$\begin{aligned}\left[\epsilon_e^{*h}\right] &= \left[{\epsilon_L}_e^{*h}\right] + \left[{\epsilon_{NL}}_e^{*h}\right] \\ \left[{\epsilon_e}^h\right] &= \left[{\epsilon_L}_e^h\right] + \left[{\epsilon_{NL}}_e^h\right]\end{aligned} \tag{20}$$

The geometrically non-linear formulation now considered is based on Von-Karmann assumptions where deflexion is moderately large, while rotations and strains remain small. Non-linear virtual strain rate matrix in Eq. (20) is then given by :

$$\begin{aligned}\left[{\epsilon_{NL}}_e^{*h}\right]^T = [\; & \frac{1}{2}({v_3}^h{}_{,1} + b_1^\alpha {v_\alpha}^h)({v_3}^{*h}{}_{,1} + b_1^\alpha {v_\alpha}^{*h}) \quad \frac{1}{2}({v_3}^h{}_{,2} + b_2^\alpha {v_\alpha}^h)({v_3}^{*h}{}_{,2} + b_2^\alpha {v_\alpha}^{*h}) \\ & ({v_3}^h{}_{,1} + b_1^\alpha {v_\alpha}^h)({v_3}^{*h}{}_{,2} + b_2^\lambda {v_\lambda}^{*h}) + ({v_3}^h{}_{,2} + b_2^\alpha {v_\alpha}^h)({v_3}^{*h}{}_{,1} + b_1^\lambda {v_\lambda}^{*h}) \\ & 0 \quad 0 \;]\end{aligned} \tag{21}$$

and non-linear strain matrix is :

$$\left[\epsilon_{NLe}{}^h\right]^T = [\ \frac{1}{2}({v_3}^h{}_{,1} + b_1^\alpha {v_\alpha}^h)^2 \quad \frac{1}{2}({v_3}^h{}_{,2} + b_2^\alpha {v_\alpha}^h)^2 \quad ({v_3}^h{}_{,1} + b_1^\alpha {v_\alpha}^h)({v_3}^h{}_{,2} + b_2^\lambda {v_\lambda}^h) \quad 0 \quad 0\ ] \tag{22}$$

4.4.1 Consistent linearization procedure

From these last equations, it is evident that Eq. (19) is non-linear with respect to displacements, and a Newton algorithm has to be used to find a numerical solution of Eq. (18). For a Newton-type method, knowledge of the tangent stiffness is required and can be derived using standard linearization procedures. Applying it to Eq. (18), we obtain :

$$J(\vec{u}^h, \vec{u}^{*h})_{\cup\Omega_e(0)} = J(\vec{\bar{u}}^h, \vec{u}^{*h})_{\cup\Omega_e(0)} + D_{\vec{u}} J(\vec{\bar{u}}^h, \vec{u}^{*h}).\Delta\vec{u}^h \tag{23}$$

with $\vec{u}^h = \vec{\bar{u}}^h + \Delta\vec{u}^h$, where $\vec{\bar{u}}^h$ refers to a known state.

According to Eq. (23), the linearized form of the functional Eq. (18) is deduced and we now have to find the solution of the following equation :

$$D_{\vec{u}} a(\vec{\bar{u}}^h, \vec{u}^{*h})_{\cup\Omega_e(0)}.\Delta\vec{u}^h = -a(\vec{\bar{u}}^h, \vec{u}^{*h})_{\cup\Omega_e(0)} + f(\vec{u}^{*h})_{\cup\Omega_e(0)} + F(\vec{u}^{*h})_{\cup\mathcal{C}_e(0)}\ , \quad \forall\vec{u}^{*h} \tag{24}$$

The left member of Eq. (24) has to be computed and gives the tangent operator, while other quantities in the right member are known vectors as they depend only on the known state $\vec{\bar{u}}^h$.

4.4.2 The tangent stiffness matrix

The tangent stiffness matrix is now derived from the left member of Eq. (24). For an arbitrary finite element $\Omega_e(0)$ of the mesh $\cup\Omega_e(0)$, the tangent operator is found as :

$$\begin{aligned} D_{\vec{u}} a(\vec{\bar{u}}^h, \vec{u}^{*h})_{\Omega_e(0)}.\Delta\vec{u}^h = \ & \int_{\Omega_e(0)} \left[E_e^{*h}\right]^T [A_e] \left[\Delta {E_e}^h\right] \sqrt{a} d\Omega_e(0) + \\ & \int_{\Omega_e(0)} \left[E_e^{*h}\right]^T \left[A_e(\vec{\bar{u}}^h)\right] \left[\Delta {E_e}^h\right] \sqrt{a} d\Omega_e(0) + \\ & \int_{\Omega_e(0)} \left[E_e^{*h}\right]^T \left[A_e(\bar{\sigma}^h)\right] \left[\Delta {E_e}^h\right] \sqrt{a} d\Omega_e(0) \end{aligned} \tag{25}$$

In Eq. (25), the matrix $[A_e]$ has been given in 4.3.1 (see Eq. (15)), as well as vectors $[{E_e}^h]$ and $[\Delta {E_e}^h] = \Delta[{E_e}^h]$ from Eq. (17). The matrix $[A_e(\vec{\bar{u}}^h)]$ depends on material properties and on both linear and quadratic known state $\vec{\bar{u}}^h$. Finally, the matrix $[A_e(\bar{\sigma}^h)]$ is linked to the in-plane stresses.

Following the procedure given in 4.3.1 to derive the linear stiffness matrix $[K_e]$, it is easy to compute the tangent stiffness matrix, denoted $[K_{Te}]$, so that :

$$D_{\vec{u}} a(\vec{\bar{u}}^h, \vec{u}^{*h})_{\Omega_e(0)}.\Delta\vec{u}^h = [Q_e^*]^T [K_{Te}] [\Delta Q_e] \tag{26}$$

where

$$[K_{Te}] = [K_e] + \left[K_e(\vec{\bar{u}}^h)\right] + \left[K_e(\bar{\sigma}^h)\right] \tag{27}$$

In Eq. (27), to compute either matrix $[K_e]$ or $\left[K_e(\vec{\bar{u}}^h)\right]$ or $\left[K_e(\bar{\sigma}^h)\right]$, we use Eq. (15) respectively based either on $[A_e]$ or $[A_e(\vec{\bar{u}}^h)]$ or $[A_e(\bar{\sigma}^h)]$.

5 Numerical results on non linear test

Only buckling and post-buckling analysis are presented here. For both analysis, numerical simulations are compared with results issued from experiments. Experiment and modelisation are firstly described and results are then discussed.

Experiment : Experimental conditions are now described.

test configuration : A rectangular sandwich plate is set in a pressing-machine which permits to reach $100kN$ of compression force. Plate dimensions are : $390mm \times 200mm$. The sandwich is made of $12.7mm$ nida for core and respectively $0.55mm$ of laminated glass fibers/epoxy matrix for skins.
A mechanical kneecap joining is realized in order to ensure simply supported boundary conditions, see Fig. 1. A constant velocity of $0.9mm/mn$ for the force application is satisfied during the test.

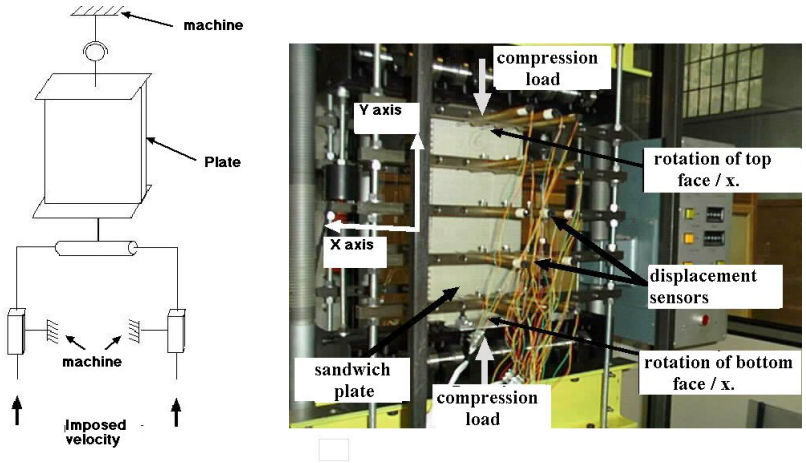

Figure 1: Experimental buckling and post-buckling.

instrumentations and measures : Critical load, displacements and strains of the plate during a test are obtained by measurements and will stand for reference values in numerical simulations.
Therefore, sensors and gages have been arranged on the plate and on the pressing-machine, see Fig. 1 for displacement sensors position.

observations : Experimental tests have been repeated for a good representation of measurements. Dispersions have been observed during experiments due to variations of initial conditions (plate preloaded or not, compression parallel or perpendicular to sheets directions). A representative test, referenced by $test12$, has been retained for later comparison with numerical simulations.

Simulations : Boundary conditions, mesh and mechanical properties used for simulations are described below :

geometry: The rectangular plate described above is modelized.

boundaries conditions and loading: The sandwich panel can rotate (see Fig. 1) from its smallest edges and is free of constraints on the others. A constant pressure is firstly imposed all over the plate to initiate bending deformed shape. So, incremental in plane compression load is applied on the two opposite edges of the panel to simulate post buckling behaviour.

mesh : Due to symmetry, only a quarter of the plate panel is modelized using $N = 1$ (two elements), $N = 2$ (four elements) and $N = 4$ (sixteen elements) meshes, see Fig. 2. Convergence have been achieved with the $N = 1$ coarse mesh for the critical buckling load and with the $N = 2$ mesh for the post buckling displacements and strains values.

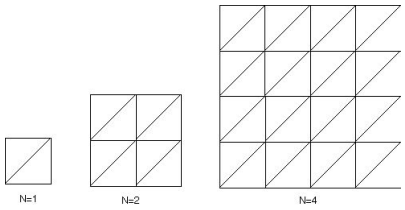

Figure 2: Discretisations $N = 1$, $N = 2$, $N = 4$.

material properties : Elastic modulus, in N/mm^2, are given in Tab. 1. In this

	E_1	E_2	E_3	G_{12}	G_{13}	G_{23}	ν_{12}
Core (Nida)	$--$	$--$	178	$--$	172	238	0.3
Skins (Glass fiber/Epoxy matrix)	21500	21500		5000	$--$	$--$	0.3

Table 1: Material properties of the sandwich plate.

table, values are issued from experimental characterization excepted for nida elastic modulus E_1, E_2 and for skins shearing modulus G_{13} and G_{23}. A sensibility analysis has proved these last material coefficients had no influence.

Results: First of all, numerical critical buckling load obtained for the present element compared with experimental values is given in Tab. 2.

	N	DOF	Critical load
Numerical values	1	55	13.20
	2	200	13.19
	4	760	13.19
Experimental value			13.35

Table 2: Critical load : experimental and numerical values.

On the other hand, numerical and experimental results for the transverse displacement v_3 and the strain components $\epsilon_{xx} = \epsilon_{11}$, $\epsilon_{yy} = \epsilon_{22}$ at the plate center are compared in Fig. 3 and Fig. 4.

Fig. 3 shows how the transverse displacement evolution is influenced by bending pre-loading of the plate. The slope of loading in the linear part can be adjusted by varying initial pressure before going on post-buckling part. The best slope correlation is conserved for strains predictions. However bending pre-loading value may be, the limit value is always in good agreement with experimental results.
Discrepancies can be observed during the linear part of the loading, see Fig. 4. Experimental results show non linear material phenomenon which occur during this loading stage. Therefore, linear material assumption employed in the model is not convenient. However, good evaluation of limit value can be obtained during the post-buckling non linear part.

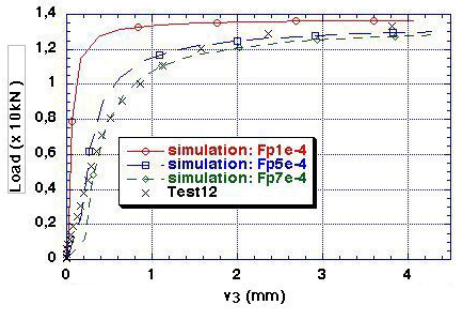

Figure 3: Evolution of transverse displacement v_3 at the plate center.

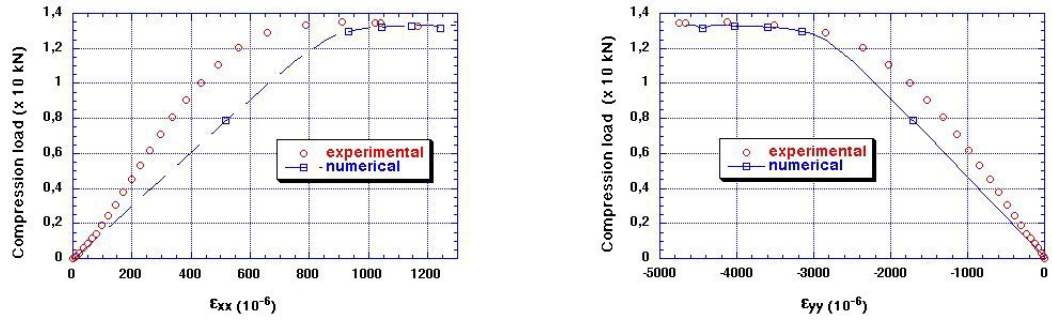

Figure 4: Evolution of strains ϵ_{xx} and ϵ_{yy}.

Finally, good evaluations of global (v_3 transverse displacement) and local values (ϵ_{xx} and ϵ_{yy}) can be obtained for a low cost (only two elements are necessary in this case) using this new element.

6 Conclusion

In this paper, a new six node multilayered triangular finite element has been presented to analyse the behaviour of composite laminated and sandwich shells. This new element :

- is based on a refined kinematic which permits to satisfy interlaminar continuity for both displacements and transverse shear stresses, and boundary conditions at the top and bottom surfaces of the shell or plate,
- uses high order polynomia to interpolate the generalized displacements : field compatibility for transverse shear strains is then assured and locking phenomenon is avoided.

Buckling and post-buckling analysis of a sandwich plate have been experimented and simulated using the present element. Comparisons between numerical and experimental values have been established and good results have been obtained for both critical load and strains evolutions. Our future work points towards investigations on non linear constitutive law in order to recover experimental results presented in previous section. Furthermore, some non linear static, buckling and post-buckling tests on multilayered shells will be considered.

References

[1] Argyris, J.H., Fried, I., Scharpf, D.W. The TUBA family of plate elements for the matrix displacement method. *Aero. J. Royal Aeronaut. Soc.*, **72**, 701–709 (1968).

[2] Béakou, A., Touratier, M. A rectangular finite element for analysing composite multilayered shallow shells in statics, vibration and buckling. *Int. Jour. Num. Meth. Eng.*, **36**, 627–653 (1993).

[3] Bernadou, M. *Finite Element Methods for Thin Shell Problems*. John Wiley and Sons (1996).

[4] Carrera, E. Theories and Finite Elements for Multilayered, Anisotropic, Composite Plates and Shells. **9**(2), 87–140 (2002).

[5] Dau, F. *A doubly curved C^1 finite shell element based on a refined model for multilayered/sandwich shell structures*. Thèse de Doctorat, ENSAM Engineering School, Paris-France (2004).

[6] Ganev, H.G., Dimitrov, Tch.T. Calculation of arch dams as a shell using an IBM-370 Computer and curved finite elements. In *Theory of shells*, pp. 691–696. North-Holland, Amsterdam (1980).

[7] Touratier, M. A refined theory of laminated shallow shells. *Int. J. Solids Struc.*, **29**(11), 1401–1415 (1992).